

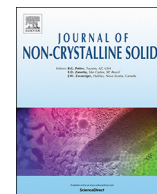
This is the peer reviewed version of the following article:

An atomic-level look at the structure-property relationship of cerium-doped glasses using classical molecular dynamics / Pedone, Alfonso; Tavanti, Francesco; Malavasi, Gianluca; Menziani, Maria Cristina. - In: JOURNAL OF NON-CRYSTALLINE SOLIDS. - ISSN 0022-3093. - 498:(2018), pp. 331-337. [10.1016/j.jnoncrysol.2018.03.040]

Terms of use:

The terms and conditions for the reuse of this version of the manuscript are specified in the publishing policy. For all terms of use and more information see the publisher's website.

19/12/2025 04:16



An atomic-level look at the structure-property relationship of cerium-doped glasses using classical molecular dynamics

Alfonso Pedone, Francesco Tavanti, Gianluca Malavasi, Maria Cristina Menziani*

Dipartimento di Scienze Chimiche e Geologiche, Università di Modena e Reggio Emilia, Via G. Campi 103, 41125 Modena, Italy

ARTICLE INFO

Keywords:

Bioactive glasses
Cerium-doped glasses
Molecular dynamics simulations
Antioxidant activity
Bioactive properties

ABSTRACT

Ce-containing bioactive glasses are of great interest in biomedical field since they exert antioxidant properties associated with low toxicity and a broad spectrum of bacteriostatic activities. The results obtained by classical molecular dynamics simulations allow the elucidation of the correlations between the effect of the inclusion of cerium doping ions into the structure of phosphosilicate and silicate bioactive glasses and their properties. The addition of small quantities of Ce to the silicate bioglass favours the depolymerisation of the silicate network with a positive effect on the ability to dissolve in body fluid. Moreover, the under coordination of both the Ce^{3+} and Ce^{4+} species in these glasses enhances their catalytic activity towards hydrogen peroxide. Conversely, the formation of cerium phosphate domains in the phosphosilicate glasses leads to detrimental effects for both the solubility and the catalytic activity of the glasses. Finally, a new quantitative view of the structure-activity relationships governing the macroscopic properties of these glasses has been obtained by means of structural descriptor that takes into account the fragmentation of the Si network and the consequent rearrangement of the modifier ions and the network destruction per cerium unit descriptor.

1. Introduction

The increasing popularity of Bioactive glasses is due both to their composition, chemically related to the bone tissue, and their unique dissolution properties in body fluids. The rate of dissolution can be tailored by modulation of the composition of the glass. Thus, critical concentrations of ionic species can be released in the surrounding physiological environment, promoting mineralisation and stimulating the growth and differentiation of osteoblasts at the genetic level.

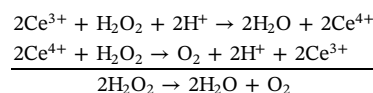
Moreover, incorporation in the glass matrix of optimal amounts of specific ions with physiological activities and therapeutic properties promotes the use of bioactive glasses in a large range of novel applications for advanced therapy in the field of soft tissue regeneration, wound healing, antimicrobial effect, drug release, cancer treatment, etc.... [1,2].

Cerium doped bioglasses have gained considerable interest in the biomedical field because of their role in enhancing osteoblastic differentiation, stimulating the production of collagen, exerting a broad spectrum of antibacterial activity and exhibiting low toxicity [3].

Our interest in this element was recently arisen from its antioxidant properties. The on-going activity of our research group in the field concerns the study of the ability of Ce-containing bioactive glasses to exert antioxidant activity by promoting the decomposition of hydrogen

peroxide (H_2O_2) and superoxide ($\text{O}_2^{\cdot-}$) radicals in vitro, as the enzymes Catalase [4] and Superoxide Dismutase [5] do at the physiological level, protecting cells from oxidative stress.

We have recently showed that, as in the CeO_2 nanoparticles on which the enzyme mimetic activity was demonstrated for the first time [6], the antioxidant activity of bioglass [7] is related to the multiple valence states of Cerium, Ce^{3+} and Ce^{4+} , which are able to catalyse the dismutation reaction of hydrogen peroxide according to the following reactions:



The relative amount of available $\text{Ce}^{3+}/\text{Ce}^{4+}$ and the kinetic of redox conversion $\text{Ce}^{3+} \leftrightarrow \text{Ce}^{4+}$ depend on the chemical nature of the glass matrix constituents and environment. In particular, the phosphate units present in the glass and/or in the physiological solution, in which the leaching and catalase mimetic activity tests are usually carried out, slow the kinetics of release and of dismutation reactions, subtracting the catalyst by forming an amorphous insoluble phase ($\text{Ce}_2\text{O}_3\text{-CePO}_4$) [8,9].

To this regards, the glass of composition $25\text{Na}_2\text{O} 25\text{CaO} 50\text{SiO}_2$ mol %, proposed by Kokubo et al. [10] is a more efficient catalyst [11].

* Corresponding author at: Via Campi 103, 41125 Modena, Italy.

E-mail address: mariacristina.menziani@unimore.it (M.C. Menziani).

<https://doi.org/10.1016/j.jnoncrysol.2018.03.040>

Received 19 January 2018; Received in revised form 23 February 2018; Accepted 17 March 2018
0022-3093/ © 2018 Elsevier B.V. All rights reserved.

However, the additional problem of determining the maximum amount of cerium oxide that can be added to the parent Kokubo glass to imprint optimal anti-oxidant ability without negatively affecting the solubility and then the bioactivity still have to be faced.

Because of their amorphous nature, there is a lack of detailed information on the microscopic structure of the bioglasses, on how the glass network is affected by the different ions making up the glass composition, and how changes in the structure affect the dissolution behaviour and the enzyme-mimetic activity. While molecular dynamic (MD) simulations will never replace laboratory experiments, it is increasingly being used to extract measurement of material properties where existing experimental techniques are unable to or where interpretation of the results of the experiment is difficult or apparently contradictory [12].

In this paper, we review the results obtained on cerium-doped bioglasses by means of the synergic experimental-computational approach developed in our laboratory and we present a new quantitative view of the structure-activity relationships governing the macroscopic properties of these glasses.

2. The glass

2.1. Glass compositions

Two series of bioactive glasses doped with variable percentages of cerium oxide have been considered for computational simulations studies of bulk materials [4,11]. Their molar compositions are reported in Fig. 1.

The parent glass of the first series, hereafter identified as H series, is the well-known 45S5 Bioglass® [13], whereas the parent glass of the second one (hereafter referred as K series) is the phosphate free glass proposed by Kokubo et al. [10]. K_5.3 is partially crystallized therefore it has not been used for subsequent analysis.

In addition, bioactive glass nanoparticles (NP) of the same composition of the bulk H_3.6 and K_3.6 glasses have also been considered in order to investigate the effect of surface area and reduced size in the structure-property relationships with respect to the bulk glasses [14].

The relative amount of Ce^{3+} and Ce^{4+} in the two series of glasses studied was determined by XPS [4] and K-edge XANES [15]. The results obtained by the first technique suggested that the amount of the Ce^{3+} and Ce^{4+} is balanced in the K glass ($\text{Ce}^{3+}/\text{Ce}^{4+} = 1.2$), while it is substantially different in the H glass ($\text{Ce}^{3+}/\text{Ce}^{4+} = 3.5$); qualitative

evidences from the second technique suggest that the $\text{Ce}^{3+}/\text{Ce}^{4+}$ ratio is not significantly dependent on the cerium doping concentration.

2.2. Glass MD simulations

The structures of the glasses have been generated through classical MD simulations by using the DL_POLY package [16]. For the molecular simulations of the bulk materials, a well-established melt-quench computational protocol, described in previous work has been used [4]. Periodic boundary conditions (PBC) were used on a cubic box of side $\sim 52 \text{ \AA}$ that contains around 10,000 atoms, depending on glass density. The total number of each Ce^{3+} and Ce^{4+} species in the final box of the H_3.6 glass is 96 and 27, respectively; whereas in the K_3.6 glass is 70 and 60, respectively.

The glass nanoparticles have been obtained by removing the PBCs and imposing spherical containing potentials, while quenching from 3200 K to 300 K, until a NP with radius of about 33 \AA was obtained [14].

Three independent simulations have been performed for each composition, the typical error associated to the results are on the second digit of the structural properties computed.

The Extended X-Ray Absorption Fine Structure (EXFAS) patterns were calculated for the BG_5.3 MD-derived three-dimensional structures using the FEFF 8 code [17]. Each EXAFS pattern was averaged over all the non-equivalent cerium atoms within the MD calculated shell (180 for BG_5.3 and 130 for K_3.6), including single and multi-scattering paths by atoms within a 9 \AA distance from the central atom.

2.3. Force field parameters

In order to obtain a reasonable good description of the short and medium-range order of the glass structure at affordable computational costs, an adiabatic core-shell model [18] was used. In this model, the polarizability of oxygen induced by the network environment is straightforwardly included by considering the forces acting on the oxygen shell by the other ions [19]. Parameters for Ce^{3+} and Ce^{4+} compatible with this force field were derived recently by fitting on the Ce-containing crystal phases available in the literature [20]. Notwithstanding the number of experimental data available for the fitting procedure were scarce, especially for the Ce^{4+} species (5 crystalline phases containing Ce^{3+} (Ce_2O_3 , $\text{CeP}_5\text{O}_{14}$, $\text{Ce}_2\text{O}_7\text{Si}_2$, CePO_4 and $\text{Al}_3\text{CeP}_2\text{O}_{14}\text{H}_6$) and 2 crystalline phases containing Ce^{4+} (CeO_2 and

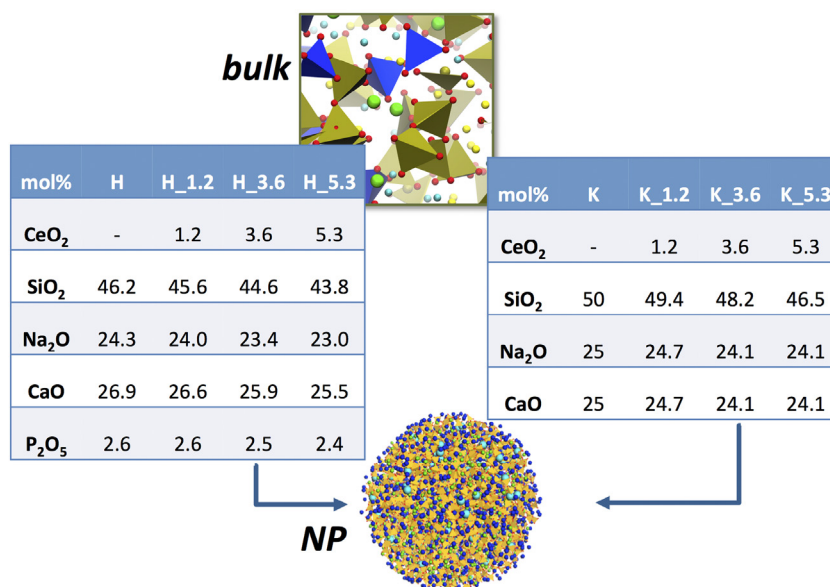


Fig. 1. The composition of the glasses studied as bulk and NP surface.

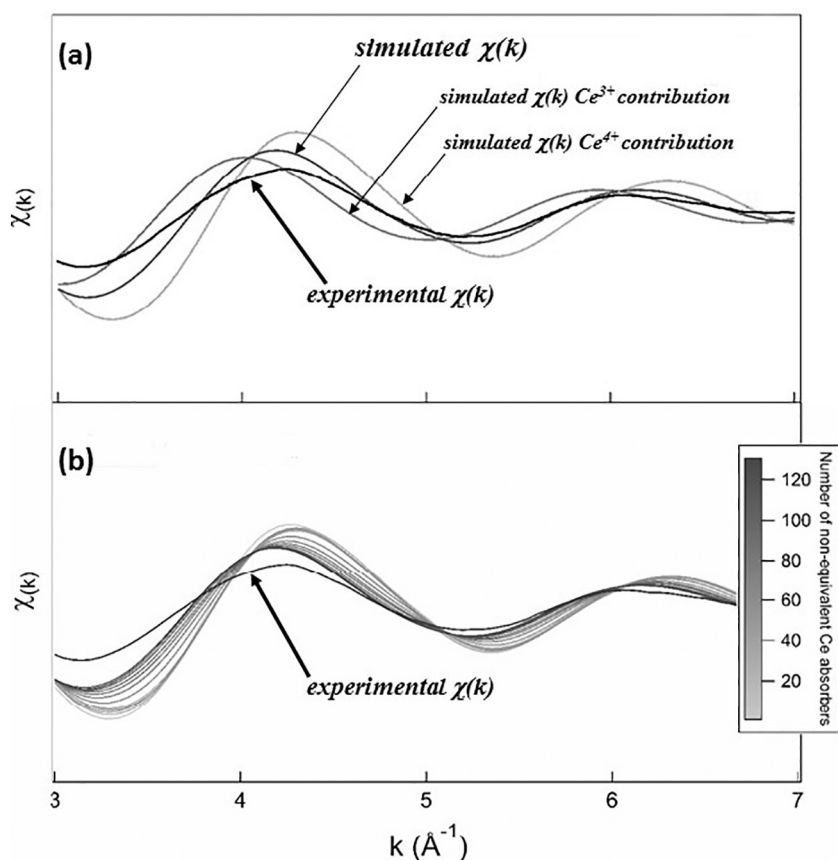


Fig. 2. (a) $\chi(k)$ simulated for the BG_5.3 glass by considering all of the cerium atoms contained in MD box, and the contribution due to the Ce^{3+} and Ce^{4+} ions. (b) Evolution of the average $\chi(k)$ simulated with increasing number of non-equivalent Ce ions in the MD box. In (a) and (b) the experimental $\chi(k)$ is reported for comparison.

CeSiO_4), the force field was found to reproduce satisfactorily the Ce^{3+} and Ce^{4+} environments in silico-phosphate and silico-aluminophosphate glasses.

3. Results and discussion

3.1. Force field validation

A valuable way to check the reliability of the intermolecular potentials used and validate MD simulation results is the comparison of the computational results obtained with the structural information derived from the EXAFS spectrum.

Recently, quantitative information on the Ce local atomic environment in samples of the same compositions analysed in the present paper have been obtained by means of Ce K-edge absorption spectra [15].

Fig. 2a shows the measured EXAFS spectrum ($\chi(k)$) of the BG_5.3 glass in the interval 3–7 \AA^{-1} superimposed to the ones simulated by considering the total amount of Cerium in the glass and the contribution of the Ce^{3+} and Ce^{4+} species. It can be appreciated that the similarity between measured and simulated spectra is maximized when both the contributions of the Ce^{3+} and Ce^{4+} ions are considered, confirming that both species are contemporaneously present in the glass. Moreover, Fig. 2(b) shows that the experimental spectrum is better reproduced by increasing the number of possible configurations of the Ce ions present in the simulation box.

Despite the limitations of the parameterization and finite size of the sample used in the MD simulation, the coordination around the Ce^{3+} and Ce^{4+} ions is reasonable well determined by the models obtained, as demonstrated by the good agreement in phase between simulated spectra and measured EXAFS signal in the range considered for first shell fitting. The finite number of non-equivalent cerium atoms in the MD models is responsible for the difference in the amplitude of the signal and the dumping at long-range disorder.

3.2. Structure-activity relationships

3.2.1. Short range order

Overall, the short-range order as detected by the bond distance, bond angles and coordination numbers of the constituting ions is not, or little, affected by the addition of cerium oxide, both in the bulk [15] and at the surface [14].

The silicon and phosphorus ions are four-coordinated in all glass compositions examined. Cerium acts as a modifier cation, being coordinated by non-bridging oxygens (NBOs) only, and strongly competes with Na and Ca ions for NBOs coordination. The Ce-O pair distribution functions in Fig. 3 show data values of full width at half maximum (FWHM) smaller for Ce^{4+} with respect to Ce^{3+} in both H and K glasses, indicating a more defined local environment for Ce^{4+} . In fact, although small amount of 6- and 8-fold coordination are found, the most probable coordination for Ce^{4+} ions is 7 (Fig. 3); whereas the 6 or 7 oxygen coordination is equally probable for Ce^{3+} . These results are in agreement with the values obtained in previous MD studies on Ce silico-phosphate and aluminosilicophosphate glasses [20,21], and Ce aluminophosphate glasses [22], as shown in Fig. 4. In all cases, a part from the PACS2 glass, the coordination number (CN) of the Ce^{4+} species is larger with respect to the one of the Ce^{3+} species, in line with the trends observed by EXAFS studies of rare earth phosphate glasses [23] and X-ray diffraction measurements performed on Ce-phosphate glasses [24]. Discrepancies in the results obtained by Du et al. [22] for the PACS2 glass could be ascribed to their use of a rigid model potential. In fact, as it has been shown for the CSP glass [19] this potential yields CN values of 6.7 and 6.5 for the Ce^{3+} and Ce^{4+} species respectively, with a reverse trend with respect to the core-shell potential (CN = 6.5 and 7.8 Ce^{3+} and Ce^{4+} species respectively).

The higher Lewis acidity of under-coordinated cerium observed in the K series (6.3–6.4 for Ce^{3+} ions; 6.7–6.8 for Ce^{4+} ions) with respect to the H series (6.5–6.6 for Ce^{3+} ions; 7.0–7.08 for Ce^{4+} ions) and at

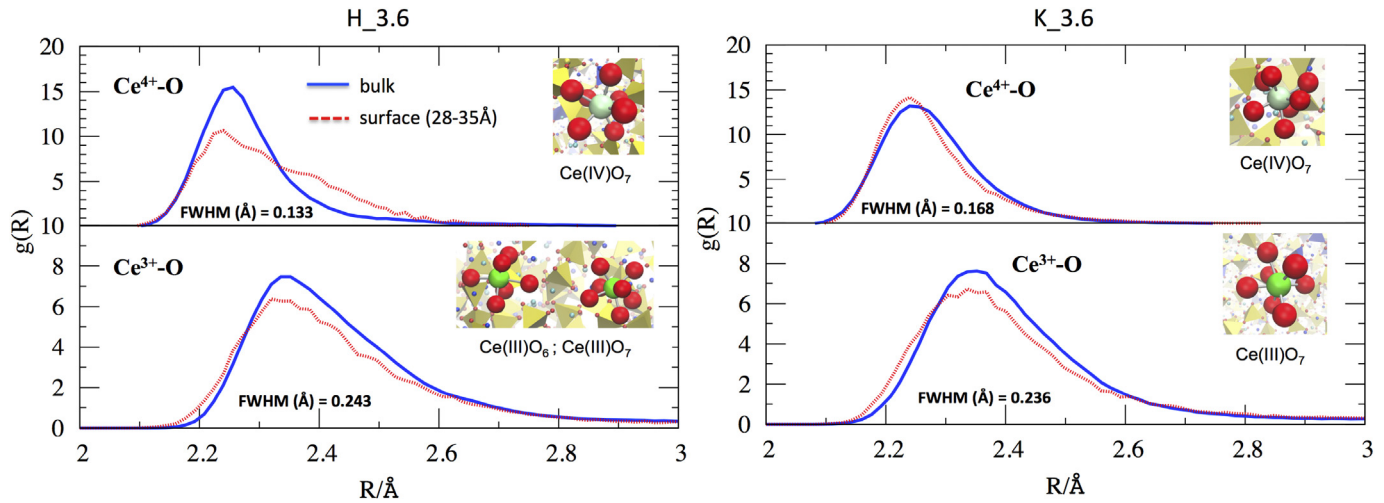


Fig. 3. Pair radial distribution functions, $g(R)$, for the Ce-O pairs in the H_{3.6} and K_{3.6} glasses. The data values of full width at half maximum (FWHM) and the typical oxygen arrangements around the Ce ions are reported.

the surface with respect to the bulk enhances its reactivity with positive consequences on its catalytic activity towards hydrogen peroxide.

Interestingly, in the H series a moderate increase of the CN of Na (5.4–6.0), is observed as a function of CeO₂ addition (Table 1). This effect, mainly due to the increment of NBOs, is less pronounced in the K series. Overall, the variation in the CN_{Ca-O} as a function of CeO₂ addition is only marginal. This picture of the short range environment of Na and Ca ions shows a nice agreement with the results of previous MD and NMR investigations on silicate glasses [23–26].

3.2.2. Medium range order: Q_n distribution

The Q_n distribution (where Q designates “quaternary” and n the number of bridging oxygens (BOs) connected to the network former cations) provides a measure to detect the effect of CeO₂ on the glass polymerization, and can be summarized in the descriptor network connectivity (NC) defined as the average number of BOs per network-forming [27,28].

The un-doped H and K glasses present a trinomial $Q_n(\text{Si})$ distribution dominated by Q_2 species (52, 56% respectively) with a similar population of Q_1 and Q_3 species (21.2%) for the K glass, whereas in the H glass the Q_3 species dominates over the Q_1 ones (Fig. 5).

The addition of CeO₂ fragments the glass structure with NC monotonically decreasing from 2.4 and 2.1 to 1.6 and 1.7 for K and H glass, respectively. In the K series, the NBOs necessary to stabilize the first coordination sphere of Ce ions are supplied by the depolymerisation of the silicate network. In fact, the population of Q_2 and Q_3 species

Table 1

Average coordination number for the modifier ions.

CN _{X-O}	H_1.2	H_3.6	H_5.3	K_1.2	K_3.6	K_5.3
Na-NBO	4.00	4.77	4.81	4.30	4.50	4.60
Na-BO	1.36	1.25	1.20	1.30	1.30	1.20
Na-O	5.36	6.02	6.01	5.60	5.80	5.80
Ca-NBO	5.35	5.40	5.41	5.06	5.20	5.14
Ca-BO	0.47	0.54	0.45	0.50	0.50	0.50
Ca-O	5.82	5.94	5.86	5.56	5.70	5.64

drastically decreases to 43.6% and 10.8%, respectively (for K_{5.3}Ce glass), whereas Q_1 increases to about 40%. The effect of CeO₂ addition on the silica network of the H series is less pronounced: phosphorus contributes significantly to supply the NBOs necessary for stabilization of the Ce species. Thus, the amount of orthophosphate (Q_0) environment in the BG glass (77%) increases to 89% after the addition of only 5.3 mol% of CeO₂.

3.2.3. Cation-cation coordination

The cation-cation coordination numbers (CN_{X-Y}) computed by integrating the first peak of the corresponding pair distribution functions provides further insights into the medium range order and chemical disorder of these glasses.

The addition of CeO₂ oxide into the H glass causes a migration of Na ions from the P environment to the Si network promoting the

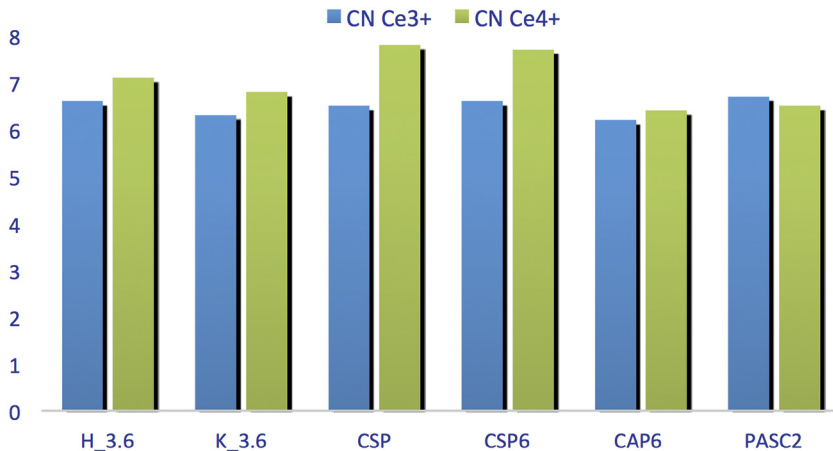


Fig. 4. Coordination number of glasses containing cerium oxide ions. H_{3.6} and K_{3.6} are the silicate glasses presented in this paper. Data for CSP (Ce₂O₃ 8%, P₂O₅ 37%, SiO₂ 55%) and CSP6 (Ce₂O₃ 18%, P₂O₅ 62%, SiO₂ 17%, Al₂O₃ 2.3%) are taken from ref. [20]. Data for CAP6 (Ce₂O₃ 13.8%, P₂O₅ 69.8%, Al₂O₃ 16.4%) are taken from ref. [22], and those for PASC2 (Ce₂O₃ 5%, P₂O₅ 71.25%, SiO₂ 9.5%, Al₂O₃ 14.25%) from ref. [21]. Glass compositions are expressed in mol%.

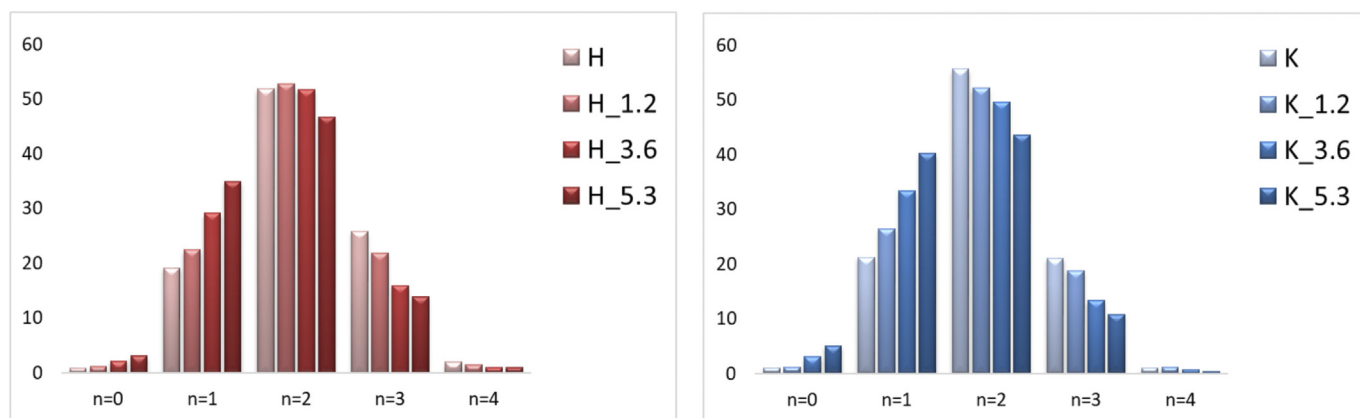


Fig. 5. Q_n (Si) distributions for the H and K series of glasses.

depolymerisation of the silica network according to the reaction: $\text{Si-O-Si} + \text{Na}_2\text{O} \rightarrow 2\text{SiONa}$.

A strong preference of Ce ions to be found in the close surrounding of the phosphate groups is accounted for by the 1.1 value of the P/Si ratio around Ce ions in the MD models, which is about 10 times higher than the nominal one (Fig. 6). This phenomenon is responsible for the reduced release of phosphate ions from the glass network in glasses doped with high concentration of Ce, and, as a consequence, of the loss of the bioactive property. In fact, a stable, insoluble CePO_4 crystalline phase can be observed by XRD analysis after thermal treatment of the glass samples [29]. Moreover, the segregation of Ce^{3+} species in cerium phosphate domains has a detrimental effect also on the catalase mimetic activity of these glasses since both Ce^{3+} and Ce^{4+} species are necessary for the catalysis of the dismutation reaction of hydrogen peroxide.

The most notable effect induced by Ce addition on the structure of the K series of glasses is observed in the surrounding of the Ce^{4+} ions: the number of Si ions around Ce^{4+} ions decreases 7.8 to 7.1. Indeed, the presence of CeO_2 crystal phases in the K_5.3 glass is observed by XRD measurements on the heat-treated glass [11].

3.2.4. Bulk vs surface distribution of modifier ions

The distribution of the modifier species in the H3.6 and K3.6 bulk glasses, with respect to the corresponding ones in the core and surface of the NP glasses is summarized in Table 2. The density ratio $\text{Ce}^{3+}/\text{Ce}^{4+}$ and $\text{Na}^+/\text{Ca}^{2+}$ is computed for the NP in a region within 28 Å from the centre of mass (core) and within a spherical shell located between 30 and 33 Å from the centre of mass (surface).

It can be noted that, in general the NP surface is significantly richer of sodium ions with respect to calcium, therefore, once in contact with body fluid, the initial dissolution process should be favoured by the nanosized particles. However, the pronounced pH increase due to the

Table 2

Ratio of the $\text{Ce}^{3+}/\text{Ce}^{4+}$ and Na/Ca modifier ions in the bulk of the H_3.6 and K_3.6 glasses, and in the core and surface of the corresponding nanoparticles.

	H_3.6 $\text{Ce}^{3+}/\text{Ce}^{4+}$	K_3.6 $\text{Ce}^{3+}/\text{Ce}^{4+}$	H_3.6 Na/Ca	K_3.6 Na/Ca
Bulk	~3.5	~1.2	1.7	1.9
Core NP	3.5	1.0	1.9	2.0
Surface NP	~13.0	~2.1	5.2	4.5

burst of Na ions exchanged with the surrounding solution can be detrimental to the cells; therefore, a careful optimization of the sodium gradient of concentration should be achieved.

Interesting, the $\text{Ce}^{3+}/\text{Ce}^{4+}$ ratio at the surface of the NP denotes an almost exclusive presence of Ce^{3+} in the H glass, whereas for the K glass the proportion of Ce^{3+} and Ce^{4+} is more balanced.

According to the results reported by Pirmohamed et al. [30] catalase mimetic activity of nanoceria is inversely related to the concentration of cerium atoms in the +3 oxidation at the surface of the nanoparticle; therefore, Ce doped K-NPs should possess better antioxidant properties compared to the ones derived by conventional bioactive glasses.

3.3. Quantitative structure-activity relationships (QSAR)

A major part of the functionality of bioactive glasses originates by their ability to dissolve in body fluid. From the experimental point of view, this property can be modelled by measuring the release of glass ions after soaking in the H_2O_2 + SBF solution for the two series of glasses. In particular, the amount of released Si, Ca and P ions for the H series, and Si and Ca for the K series after 96 h soaking (Total Leaching) are considered [11]. In fact, according to the mechanism proposed by Hench [31] the initial $\text{Na}^+/\text{H}_3\text{O}^+$ exchange and pH rise is followed by

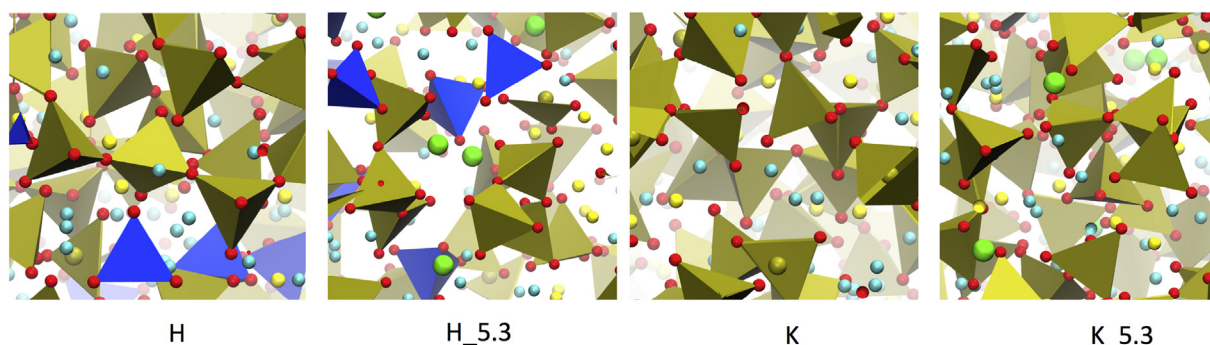


Fig. 6. The structure of in the H_5.3 and K_5.3 glasses. Si is represented in dark yellow, O in red, P in blue, Ce in green, Na light blue, and Ca light yellow. (For interpretation of the references to color in this figure legend, the reader is referred to the web version of this article.)

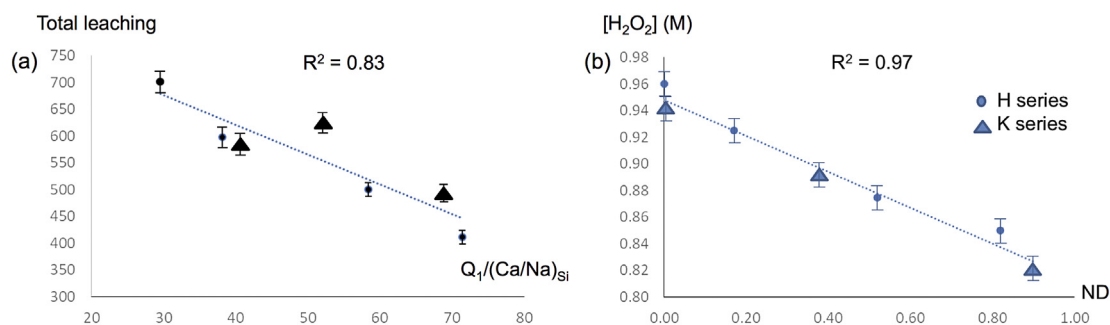


Fig. 7. (a) Correlations between the experimental Total Leaching data values (ppm) [11] and the structural descriptor $Q_1/(Ca/Na)_{Si}$. The linear regression obtained is: Total Leaching = $5.54 Q_1/(Ca/Na)_{Si} + 825.35$ $n = 7$, $R^2 = 0.83$. (b) Correlations between the experimental concentration of H_2O_2 (M) data values [4,11] and the ND descriptor. The linear regression obtained is: $[H_2O_2] = -0.13 ND + 0.95$ $n = 7$, $R^2 = 0.97$.

alkaline hydrolysis of Si-O-Si bonds and subsequent formation of a silica gel layer by condensation reactions between Si-OH groups. The presence of a silica gel layer is thought to aid hydroxyapatite $Ca_5(PO_4)_3OH$ nucleation.

Suitable structural markers to predict and compare the bioactivity of different glass compositions are related to network connectivity which, as shown by the atomic level picture derived by MD simulations, depends, in a non-trivial way, both on the amount and nature of network forming and modifier ions [32].

Fig. 7a shows the linear correlation obtained between the experimental Total leaching after 96 h soaking in a $H_2O_2 + SBF$ solution, and the $Q_1/(Ca/Na)_{Si}$ descriptors derived by the MD simulations. The total amount of released Si, Ca, and P ions is considered for the H series of glasses, whereas, for the K series, only the released Si, Ca ions are summed up.

In both series the ion release in solution decreases as the content of Cerium increases, this phenomenon is well accounted for ($R^2 = 0.828$) by considering that the fragmentation of the Si network (Q_1) occurs with a variation in the segregation of Na and Ca ions by the silica network induced by cerium addition to the two series of glasses. ($Ca/Na)_{Si}$ is the ratio between the number of Ca and Na in the second coordination sphere of Si compared it to the Ca/Na ratio in the nominal glass composition).

The ability of Ce-containing bioactive glasses to inhibit oxidative stress has been tested in vitro in terms of reduction of the concentration of hydrogen peroxide observed after glass soaking. The degradation of hydrogen peroxide is cerium dependent, increasing as cerium content increases in the glasses. Classical molecular simulations cannot provide descriptors related to the interconversion between Ce^{3+} and Ce^{4+} , which is a redox reaction of fundamental importance for the exhibition of catalase mimetic activity. However, the results of classical molecular simulations provide elements for a direct or indirect estimation of the availability of Cerium on the glass surface. Qualitative considerations have been presented in the previous paragraphs. From a quantitative point of view, the network destruction per cerium unit (ND) descriptor explains 97% of the variation in the degradation of hydrogen peroxide (Fig. 7b). The main contribution to this descriptor is given by the amount of Q_1 species, since, as shown in Fig. 5, it is the most responsive to Ce addition. Therefore, the availability of Cerium on the glass surface, favoured by a disrupted silicate network, regulates the amount reactive Cerium available for H_2O_2 decomposition; to this regard, the K_{3.6} shows the same catalytic efficiency than H_{5.3} (residual H_2O_2 concentration 0.85 M vs. 0.82 M, respectively).

It is worth noting that an advantage of the descriptors used in the QSPR models obtained rests in their ability to gather in a single monovariate model two series of glasses structurally significantly different. In this way, the limitation due to an insufficient number of data in the dataset is overcome. This is particularly important in these glasses, where the range of compositions is limited by the occurrence of crystallization and phase separation.

4. Conclusions and perspective

The results obtained by classical molecular dynamics simulations allow the elucidation of the effect of the inclusion of cerium doping ions on the structure and properties of bioactive glasses. In particular, significant differences are observed in the glasses, depending on the presence of phosphate ions in their compositions.

In the K series, the first coordination sphere of Ce ions is stabilized by the NBOs supplied by the depolymerisation of the silicate network, as detected by the rapid increases of the Si Q_1 species upon Ce addition. Conversely, in the H series phosphorus contributes significantly to the stabilization of the Ce^{3+} species providing an environment rich of orthophosphate (Q_0) units. This phenomenon is seminal for the reduced release of phosphate ions from the network of H glasses doped with high concentration of Ce, and, as a consequence, for the loss of the bioactive property. Moreover, the catalase mimetic activity of these glasses is also negatively affected by the formation of cerium phosphate domains, which perturb the equilibrium of the Ce^{3+} and Ce^{4+} species necessary for the catalysis of the hydrogen peroxide dismutation reaction.

Interesting, the most notable effect of Ce addition on the structure of the K series of glasses is the reduction of the Si ions in the surrounding of the Ce^{4+} ions, which may be responsible for the precipitation of CeO_2 crystal phases in glasses with high cerium content (K_{5.3} glass).

In addition, the CN of cerium in the K series is smaller with respect to those of the H series for both the Ce^{3+} and Ce^{4+} species. This phenomenon is amplified at the surface of the nanoparticles, but it is significant also in the bulk structures. The presence of under coordinated Cerium ions with high Lewis acidity in the K series of glasses affects positively their catalytic activity towards hydrogen peroxide.

Finally, the atomic level picture derived by MD simulations has allowed the derivation of suitable descriptors to obtain sound QSAR models for the quantitative rationalization of the leaching ability of the glasses in $H_2O_2 + SBF$ solution and the ability to reduce the concentration of hydrogen peroxide observed after glass soaking. In the first case, the 83% of the variance is explained by a structural descriptor that takes into account the fragmentation of the Si network and the consequent rearrangement of the modifier ions; in the second case, 97% of the variance is explained by the network destruction per cerium unit descriptor.

Although the results obtained are of help in the tailoring of specific ion release from bioactive glasses to match clinical requirements, some important challenges have still to be faced. Some of these are strictly connected to the inclusion in the glass matrix of ions with multiple oxidation states, i.e. Cerium whose local site interconversion cannot be directly accounted for by classical force fields. Other, more general ones, concern a rigorous investigation of surface reactivity both of flat and nanoparticle surfaces in water and SBF. Finally, the study of the interaction of glass surface with model systems of blood plasma proteins is mandatory to have information on the fate of glass particles

with specific medical properties once in contact with blood stream.

A promising perspective in these fields is given by the use of reactive potentials that offer an alternative method to simulate structures and chemical reactions with high accuracy, within a MD framework [33,34]. The penalty in computational efficiency is relatively small, but parametrization is hard and it is only available for the silica/water system. Therefore, the development of general and accurate reactive force fields for multicomponent oxide glasses is urgently needed.

Funding

This work was supported by a grant from the University of Modena and Reggio Emilia (FAR2017) entitled “The role of cerium oxidation state in bioactive glasses used as biomaterials of 3rd generation”.

References

- [1] A. Hoppe, N.S. Güldal, A.R. Boccaccini, A review of the biological response to ionic dissolution products from bioactive glasses and glass-ceramics, *Biomaterials* 32 (2011) 2757–2774, <http://dx.doi.org/10.1016/j.biomaterials.2011.01.004>.
- [2] V. Miguez-Pacheco, L.L. Hench, A.R. Boccaccini, Bioactive glasses beyond bone and teeth: emerging applications in contact with soft tissues, *Acta Biomater.* 13 (2015) 1–15, <http://dx.doi.org/10.1016/j.actbio.2014.11.004>.
- [3] B.R. Barrioni, A.A.R. de Oliveira, M. de Pereira, The evolution, control, and effects of the compositions of bioactive glasses on their properties and applications, *Biocompatible Glas*, Springer, Cham, 2016, pp. 85–117, http://dx.doi.org/10.1007/978-3-319-44249-5_4.
- [4] V. Nicolini, E. Gambuzzi, G. Malavasi, L. Menabue, M.C. Menziani, G. Lusvardi, A. Pedone, F. Benedetti, P. Luches, S. D'Addato, S. Valeri, Evidence of catalase mimetic activity in $\text{Ce}^{3+}/\text{Ce}^{4+}$ doped bioactive glasses, *J. Phys. Chem. B* 119 (2015) 4009–4019, <http://dx.doi.org/10.1021/jp511737b>.
- [5] V. Nicolini, G. Malavasi, L. Menabue, G. Lusvardi, F. Benedetti, S. Valeri, P. Luches, Cerium-doped bioactive 45S5 glasses: spectroscopic, redox, bioactivity and biocatalytic properties, *J. Mater. Sci.* 52 (2017) 8845–8857, <http://dx.doi.org/10.1007/s10853-017-0867-2>.
- [6] A. Kumar, S. Das, P. Munusamy, W. Self, D.R. Baer, D.C. Sayle, S. Seal, Behavior of nanocerium in biologically-relevant environments, *Environ. Sci. Nano.* 1 (2014) 516–532, <http://dx.doi.org/10.1039/C4EN00052H>.
- [7] L.L. Hench, R.J. Splinter, W.C. Allen, T.K. Greenlee, Bonding mechanisms at the interface of ceramic prosthetic materials, *J. Biomed. Mater. Res.* 5 (1971) 117–141, <http://dx.doi.org/10.1002/jbm.820050611>.
- [8] C. Leonelli, G. Lusvardi, G. Malavasi, L. Menabue, M. Tonelli, Synthesis and characterization of cerium-doped glasses and in vitro evaluation of bioactivity, *J. Non-Cryst. Solids* 316 (2003) 198–216, [http://dx.doi.org/10.1016/S0022-3093\(02\)01628-9](http://dx.doi.org/10.1016/S0022-3093(02)01628-9).
- [9] R.N. McCormack, P. Mendez, S. Barkam, C.J. Neal, S. Das, S. Seal, Inhibition of Nanocerium's catalytic activity due to Ce^{3+} site-specific interaction with phosphate ions, *J. Phys. Chem. C* 118 (2014) 18992–19006, <http://dx.doi.org/10.1021/jp500791j>.
- [10] H.-M. Kim, F. Miyaji, T. Kokubo, C. Ohtsuki, T. Nakamura, Bioactivity of Na2O-CaO-SiO2 glasses, *J. Am. Ceram. Soc.* 78 (1995) 2405–2411, <http://dx.doi.org/10.1111/j.1151-2916.1995.tb08677.x>.
- [11] V. Nicolini, E. Varini, G. Malavasi, L. Menabue, M.C. Menziani, G. Lusvardi, A. Pedone, F. Benedetti, P. Luches, The effect of composition on structural, thermal, redox and bioactive properties of Ce-containing glasses, *Mater. Des.* 97 (2016) 73–85, <http://dx.doi.org/10.1016/j.matdes.2016.02.056>.
- [12] C. Massobrio, J. Du, M. Bernasconi, P.S. Salmon (Eds.), *Molecular dynamics simulations of disordered materials*, Springer International Publishing, Cham, 2015, <http://dx.doi.org/10.1007/978-3-319-15675-0>.
- [13] L.L. Hench, Bioceramics: from concept to clinic, *J. Am. Ceram. Soc.* 74 (1991) 1487–1510, <http://dx.doi.org/10.1111/j.1151-2916.1991.tb07132.x>.
- [14] A. Pedone, F. Muniz-Miranda, A. Tilocca, M.C. Menziani, The antioxidant properties of Ce-containing bioactive glass nanoparticles explained by molecular dynamics simulations, *Biomed. Glas.* 2 (2016), <http://dx.doi.org/10.1515/bglass-2016-0003>.
- [15] F. Benedetti, P. Luches, S. D'Addato, S. Valeri, V. Nicolini, A. Pedone, M.C. Menziani, G. Malavasi, Structure of active cerium sites within bioactive glasses, *J. Am. Ceram. Soc.* 100 (2017) 5086–5095, <http://dx.doi.org/10.1111/jace.15049>.
- [16] W. Smith, T.R. Forester, DL-POLY 2.0: a general-purpose parallel molecular dynamics simulation package, *J. Mol. Graph.* 7855 (1996) 136–141.
- [17] A.L. Ankudinov, B. Ravel, J.J. Rehr, S.D. Conradson, Real-space multiple-scattering calculation and interpretation of X-ray-absorption near-edge structure, *Phys. Rev. B* 58 (1998) 7565–7576, <http://dx.doi.org/10.1103/PhysRevB.58.7565>.
- [18] B. Dick, A. Overhauser, Theory of the dielectric constants of alkali halide crystals, *Phys. Rev.* 112 (1958) 90–103, <http://dx.doi.org/10.1103/PhysRev.112.90>.
- [19] A. Tilocca, N.H. De Leeuw, A.N. Cormack, Shell-model molecular dynamics calculations of modified silicate glasses, *Phys. Rev. B: Condens. Matter Mater. Phys.* 73 (2006), <http://dx.doi.org/10.1103/PhysRevB.73.104209>.
- [20] E. Gambuzzi, A. Pedone, On the structure of Ce-containing silicophosphate glasses: a core-shell molecular dynamics investigation, *Phys. Chem. Chem. Phys.* 16 (2014) 21645–21656, <http://dx.doi.org/10.1039/C4CP02577F>.
- [21] J. Du, L. Kokou, J.L. Rygel, Y. Chen, C.G. Pantano, R. Woodman, J. Belcher, Structure of cerium phosphate glasses: molecular dynamics simulation, *J. Am. Ceram. Soc.* 94 (2011) 2393–2401, <http://dx.doi.org/10.1111/j.1551-2916.2011.04514.x>.
- [22] L. Kokou, J. Du, Short- and medium-range structures of cerium aluminophosphate glasses: a molecular dynamics study, *J. Non-Cryst. Solids* 403 (2014) 67–79, <http://dx.doi.org/10.1016/j.jnoncrysol.2014.07.014>.
- [23] A. Tilocca, A.N. Cormack, N.H. de Leeuw, The structure of bioactive silicate glasses: new insight from molecular dynamics simulations, *Chem. Mater.* 19 (2007) 95–103, <http://dx.doi.org/10.1021/cm061631g>.
- [24] J.K. Christie, A. Pedone, M.C. Menziani, A. Tilocca, Fluorine environment in bioactive glasses: *ab Initio* molecular dynamics simulations, *J. Phys. Chem. B* 115 (2011) 2038–2045, <http://dx.doi.org/10.1021/jp110788h>.
- [25] E. Gambuzzi, T. Charpentier, M.C. Menziani, A. Pedone, Computational interpretation of ^{23}Na MQMAS NMR spectra: a comprehensive investigation of the Na environment in silicate glasses, *Chem. Phys. Lett.* 612 (2014) 56–61, <http://dx.doi.org/10.1016/j.cplett.2014.08.004>.
- [26] E. Gambuzzi, A. Pedone, M.C. Menziani, F. Angeli, P. Florian, T. Charpentier, Calcium environment in silicate and aluminosilicate glasses probed by ^{43}Ca MQMAS NMR experiments and MD-GIPAW calculations, *Solid State Nucl. Magn. Reson.* (2015), <http://dx.doi.org/10.1016/j.snmr.2015.04.003>.
- [27] Z. Strnad, Role of the glass phase in bioactive glass-ceramics, *Biomaterials* 13 (1992) 317–321, [http://dx.doi.org/10.1016/0142-9612\(92\)90056-T](http://dx.doi.org/10.1016/0142-9612(92)90056-T).
- [28] A. Tilocca, A.N. Cormack, Structural effects of phosphorus inclusion in bioactive silicate glasses, *J. Phys. Chem. B* 111 (2007) 14256–14264, <http://dx.doi.org/10.1021/jp075677o>.
- [29] Synthesis and characterization of cerium-doped glasses and in vitro evaluation of bioactivity, *J. Non-Cryst. Solids* 316 (2003) 198–216, [http://dx.doi.org/10.1016/S0022-3093\(02\)01628-9](http://dx.doi.org/10.1016/S0022-3093(02)01628-9).
- [30] T. Pirmohamed, J.M. Dowding, S. Singh, B. Wasserman, E. Heckert, A.S. Karakoti, J.E.S. King, S. Seal, W.T. Self, Nanocerium exhibit redox state-dependent catalase mimetic activity, *Chem. Commun.* 46 (2010) 2736, <http://dx.doi.org/10.1039/b920204k>.
- [31] L.L. Hench, Bioceramics, *J. Am. Ceram. Soc.* 81 (1988) 1705–1728, <http://dx.doi.org/10.1111/j.1151-2916.1998.tb02540.x>.
- [32] D.S. Brauer, Bioactive glasses-structure and properties, *Angew. Chem. Int. Ed.* 54 (2015) 4160–4181, <http://dx.doi.org/10.1002/anie.201405310>.
- [33] J.M. Rimsza, J. Yeon, A.C.T. van Duin, J. Du, Water-nanoporous silica interactions: comparison of ReaxFF and *ab initio* based molecular dynamics simulations, *J. Phys. Chem. C* 120 (2016) 24803–24816, <http://dx.doi.org/10.1021/acs.jpcc.6b07939>.
- [34] J.M. Rimsza, J. Du, Interfacial structure and evolution of the water-silica gel system by reactive force-field-based molecular dynamics simulations, *J. Phys. Chem. C* 121 (2017) 11534–11543, <http://dx.doi.org/10.1021/acs.jpcc.7b02734>.